International Journal of Solids and Structures 45 (2008) 5181–5188

Contents lists available at ScienceDirect

International Journal of Solids and Structures

journal homepage: www.elsevier.com/locate/ijsolstr

Effect of *T*-stress on crack growth under mixed mode I–III loading

Viggo Tvergaard *

Department of Mechanical Engineering, Solid Mechanics, Technical University of Denmark, Building 404, DK-2800 Kgs, Lyngby, Denmark

ARTICLE INFO

Article history:
Received 28 January 2008
Received in revised form 6 May 2008
Available online 3 June 2008

Keywords:
Plasticity
Crack growth
T-Stress
Mixed-mode fracture
Finite strains

ABSTRACT

For a crack subjected to combined mode I and III loading the influence of a *T*-stress is analyzed, with focus on crack growth. The solid is a ductile metal modelled as elastic–plastic, and the fracture process is represented in terms of a cohesive zone model. The analyzes are carried out for conditions of small scale yielding, with the elastic solution applied as boundary conditions on the outer edge of the region analyzed. For several combinations of the stress intensity factors K_I and K_{III} and the *T*-stress crack growth resistance curves are calculated numerically in order to determine the fracture toughness. In all situations it is found that a negative *T*-stress adds to the fracture toughness, whereas a positive *T*-stress has rather little effect. For given values of K_I and *T* the minimum fracture toughness corresponds to $K_{III} = 0$.

1. Introduction

Cohesive zone models have been applied in a number of studies to calculate crack growth resistance curves for ductile solids, by using the cohesive zone model to characterize the fracture process while an elastic–plastic material model for the surrounding material is used to represent the ductility. For materials under plane strain conditions this approach has been used to study mode I cracks in homogeneous materials (Tvergaard and Hutchinson, 1992) or interface cracks between dissimilar materials under mixed mode I–mode II loading conditions (Tvergaard and Hutchinson, 1993; Tvergaard, 2001). As observed in experiments (Cao and Evans, 1989; Liechti and Chai, 1992; O'Dowd et al., 1992), the analyses predict a much increased fracture toughness when there is a significant contribution from mode II loading near the crack tip.

For conditions of small-scale yielding the effect of the non-singular *T*-stress acting parallel to the crack plane has been studied by Betegon and Hancock (1991) and Du and Hancock (1991), who found that the fracture toughness is increased by a negative *T*-stress. An approach that also applies to fully yielded specimens has been proposed by O'Dowd and Shih (1991, 1992) in the form of a two-term expansion of the plastic crack-tip fields with the first term characterized by the applied *J* and with an amplitude *Q* of the second term. The effect relies on the significant influence of a *T*-stress on the shape and size of the plastic zone at the crack-tip (Larsson and Carlsson, 1973; Rice, 1974). The approach of using a cohesive zone model to represent crack growth in a homogeneous elastic–plastic solid under mode I loading has been extended by Tvergaard and Hutchinson (1994) to account for a *T*-stress and it has been found that this method predicts a *T*-stress dependence of the fracture toughness qualitatively similar to the dependence that has been observed experimentally, e.g., in the study of Hancock et al. (1991).

In a recent study of interface delamination (Tvergaard and Hutchinson, 2008) the effect of a mode III contribution has been investigated by using a version of the cohesive zone model that accounts for tangential separation in two perpendicular directions, in addition to normal separation. The numerical analyses were based on special planar elements that incorporate the out-of-plane displacements needed to describe the mode III crack growth. This computational procedure is used here to

* Tel.: +45 4525 4273; fax: +45 4593 1475.
E-mail address: viggo@mek.dtu.dk

0020-7683/$ - see front matter © 2008 Elsevier Ltd. All rights reserved.
doi:10.1016/j.ijsolstr.2008.05.014

analyze the effect of a T-stress in a homogeneous elastic–plastic material when mode III loading is applied in addition to mode I. Thus, the present study can be considered an extension of that in Tvergaard and Hutchinson, 1994 to also account for mode III loading.

2. Problem formulation

The crack growth analyses under mixed mode I and III loading are carried out for conditions of small-scale yielding. The material is elastic–plastic, with the elastic properties E and ν, the uniaxial yield stress σ_Y and the strain hardening exponent N. This material is described by a finite strain generalization of J_2-flow theory (Hutchinson, 1973), with the uniaxial true stress-natural strain curve represented by a piecewise power law

$$\varepsilon = \begin{cases} \frac{\sigma}{E} & \sigma \leqslant \sigma_Y \\ \frac{\sigma_Y}{E}\left(\frac{\sigma}{\sigma_Y}\right)^{1/N} & \sigma > \sigma_Y \end{cases} \tag{1}$$

The small strain linear elastic solution gives the following in-plane stress components near the crack-tip

$$\sigma_{\alpha\beta} = \frac{K_I}{\sqrt{2\pi r}} f_{\alpha\beta}(\theta) + T\delta_{1\alpha}\delta_{1\beta} \tag{2}$$

where (r, θ) are polar coordinates, δ_{ij} is Kronecker's delta and T is a non-singular stress term acting parallel to the crack plane. The elastic stresses corresponding to the mode III problem are uncoupled to the in-plane components (2), and the corresponding tractions on the crack plane are

$$\sigma_{23} = K_{\mathrm{III}}(2\pi r)^{-1/2} \tag{3}$$

In the analyses the T-stress is applied first, together with the corresponding transverse stress $\sigma_{33} = \nu T$ (when the transverse strain remains $\varepsilon_{33} = 0$). This uniform T-stress field is kept below the yield limit. Subsequently, displacements on the outer circular boundary are increased incrementally according to the singular K_{I} and K_{III} fields. The relation between the energy release rate and the magnitudes of the stress intensity factors is given by

$$G = \frac{1-\nu^2}{E}K_{\mathrm{I}}^2 + \frac{1}{2\mu}K_{\mathrm{III}}^2 \tag{4}$$

where μ is the elastic shear modulus.

The x_1-axis is in the crack plane and the initial crack-tip is located at $x_1 = x_2 = 0$. The traction–separation relation used to model the fracture process is specified everywhere on the boundary $x_1 > 0$, $x_2 = 0$ of the region analyzed, while zero tractions are specified for $x_1 \leqslant 0, x_2 = 0$. The traction–separation law used by Tvergaard and Hutchinson, 1993 is a special version of that proposed by Tvergaard (1990) as a generalization of the model of Needleman (1987). The version of the model used here accounts for tangential separation in two perpendicular directions, so that δ_n, δ_{t1} and δ_{t3} denote the normal and tangential components of the relative displacement of the crack faces across the interface in the zone where the fracture processes occur (Fig. 1), with δ_{t3} specifying the tangential separation parallel to the crack front (Tvergaard and Hutchinson, 2008). When δ_n^c, δ_{t1}^c and δ_{t3}^c are critical values of these displacement components and a single separation measure is defined as $\lambda = [(\delta_n/\delta_n^c)^2 + (\delta_{t1}/\delta_{t1}^c)^2 + (\delta_{t3}/\delta_{t3}^c)^2]^{1/2}$ the tractions drop to zero at $\lambda = 1$. With $\sigma(\lambda)$ displayed in Fig. 1, a potential from which the tractions are derived is defined as

$$\Phi(\delta_n, \delta_{t1}, \delta_{t3}) = \delta_n^c \int_0^\lambda \sigma(\lambda')d\lambda' \tag{5}$$

The normal component and the two tangential components of the traction acting on the interface in the fracture process zone are given by

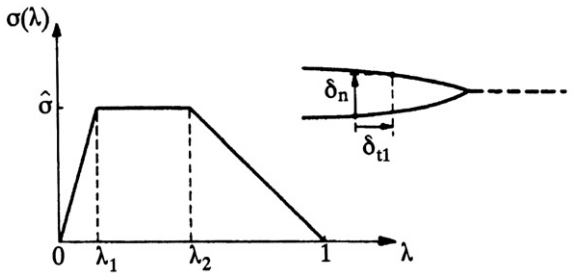

Fig. 1. Specification of traction–separation relation.

$$T_n = \frac{\partial \Phi}{\partial \delta_n} = \frac{\sigma(\lambda)}{\lambda}\frac{\delta_n}{\delta_n^c}, \quad T_{t1} = \frac{\partial \Phi}{\partial \delta_{t1}} = \frac{\sigma(\lambda)}{\lambda}\frac{\delta_{t1}}{\delta_{t1}^c}\frac{\delta_n^c}{\delta_{t1}^c}, \quad T_{t3} = \frac{\partial \Phi}{\partial \delta_{t3}} = \frac{\sigma(\lambda)}{\lambda}\frac{\delta_{t3}}{\delta_{t3}^c}\frac{\delta_n^c}{\delta_{t3}^c} \tag{6}$$

It is noted that in the problems considered here, where $K_{II} = 0$, also $\delta_{t1} = 0$ and $T_{t1} = 0$. The peak normal traction under pure normal separation is $\hat{\sigma}$, and the peak shear tractions are $(\delta_n^c/\delta_{t1}^c)\hat{\sigma}$ or $(\delta_n^c/\delta_{t3}^c)\hat{\sigma}$ in pure tangential separation in the x_1 or the x_3-directions, respectively. The work of separation per unit area of interface is given by Eq. (5) with $\lambda = 1$, and for the separation function $\sigma(\lambda)$ in Fig. 1 the work is

$$\Gamma_0 = \frac{1}{2}\hat{\sigma}\delta_n^c(1 - \lambda_1 + \lambda_2) \tag{7}$$

Tvergaard and Hutchinson (1992, 1993) and observed that the two most important parameters characterizing the fracture process in this model are Γ_0 and $\hat{\sigma}$. Scheider and Brocks (2003) have found cases where also differences in the shape of the separation law have an important effect.

For $K_{III} = 0$ a reference stress intensity factor is defined as $K_0 = [E\Gamma_0/(1-\nu^2)]^{1/2}$ and a corresponding reference length quantity R_0, which scales with the size of the plastic zone, is defined by

$$R_0 = \frac{1}{3\pi}\left(\frac{K_0}{\sigma_{Y1}}\right)^2 = \frac{1}{3\pi}\frac{E\Gamma_0}{(1-\nu^2)\sigma_{Y1}^2} \tag{8}$$

3. Numerical method

A Lagrangian convected coordinate formulation of the field equations is used, with a material point identified by the coordinates x_i in the reference configuration, accounting for finite strains. The contravariant components of the Cauchy stress tensor σ^{ij} and the Kirchhoff stress tensor τ^{ij} are related by $\tau^{ij} = \sqrt{G/g}\sigma^{ij}$. The metric tensors in the current and reference configurations are denoted by G_{ij} and g_{ij}, with the determinants G and g, respectively, and the incremental stress–strain relationship is of the form $\dot{\tau}^{ij} = L^{ijkl}\dot{\eta}_{kl}$, where L^{ijkl} are the instantaneous moduli.

The Lagrangian strain tensor is given by

$$\eta_{ij} = \frac{1}{2}(u_{i,j} + u_{j,i} + u^k_{,i}u_{k,j}) \tag{9}$$

where u^i are the displacement components on the reference base vectors and $()_{,j}$ denotes covariant differentiation in the reference frame. Numerical solutions are obtained by a linear incremental solution procedure, based on an expansion of the principle of virtual work about the current state

$$\int_V \{\Delta\tau^{ij}\delta\eta_{ij} + \tau^{ij}\Delta u^k_{,i}\delta u_{k,j}\}\mathrm{d}V = \int_A \Delta T^i \delta u_i \mathrm{d}A - \left[\int_V \tau^{ij}\delta\eta_{ij}\mathrm{d}V - \int_A T^i\delta u_i \mathrm{d}A\right] \tag{10}$$

Here, V and A are the volume and surface of the body in the reference configuration, respectively, $\Delta\tau^{ij}$ and $\Delta\ \eta_{ij}$ are the stress and strain increments, T^i are contravariant components of the nominal surface tractions, etc. The bracketed terms are equilibrium corrections. The displacement fields are approximated in terms of special planar 8-noded isoparametric elements, with three degrees of freedom in each nodal point, but with the transverse strain in the x_3-direction taken to be zero. This 8-noded planar element is similar to the usual 8-noded plane strain element, but the u_3-displacement is added as an extra degree of freedom in each nodal point, with the constraint that all displacement fields are independent of the x_3-coordinate. This means that non-zero values of η_{13} and η_{23} are allowed for, while $\eta_{33} = 0$ is enforced. The volume integral in Eq. (10) is carried out by using 2×2 integration points within each element.

A circular region with radius A_o is analyzed numerically. Actually, it would be only necessary to analyze half of this region, e.g., the half above the crack plane, since all fields are symmetric or anti-symmetric about this plane. Fig. 2 illustrates the initial near-tip mesh in the centre of the region analyzed, with 80×4 uniform quadrilaterals along the interface in the range where crack growth is studied. The length of one square element inside the uniform mesh is denoted Δ_0, and the initial crack tip is located at $x_1 = 0$. The outer radius is chosen to be $A_0 = 800{,}000\Delta_o$, which keeps the plastic zone size much smaller than $A_0/10$.

4. Results

The analyses of crack growth carried out here consider an elastic–plastic material with $\sigma_Y/E = 0.003$, $\nu = 0.3$ and $N = 0.1$. In the traction–separation law the values $\delta_n^c/\delta_{t1}^c = 1$, $\delta_n^c/\delta_{t2}^c = 1$, $\delta_n^c = 0.1\Delta_0$, $\lambda_1 = 0.15$ and $\lambda_2 = 0.50$ are used, while $\hat{\sigma}/\sigma_Y$ is varied. Also, in all the cases analyzed, the load is applied in such a manner that the stress intensity ratio K_{III}/K_I remains constant. The load is applied on the outer boundary in the form of displacements according to the elastic singularity field.

Examples of crack growth resistance curves are shown in Fig. 3 for a fixed value of the T-stress, $T/\sigma_Y = -0.5$, but for different values of the stress intensity ratio K_{III}/K_I. Here, $\hat{\sigma}/\sigma_Y = 2.4$, which gives the following value of the reference size of the plastic zone relative to the near-tip mesh size, $R_o/\Delta_o = 6.30$. During crack growth the plastic zone size is mostly 5 to 10 times R_o and the plastic fields are well resolved by the mesh applied. The curves show the energy release rate G according to (4) vs.

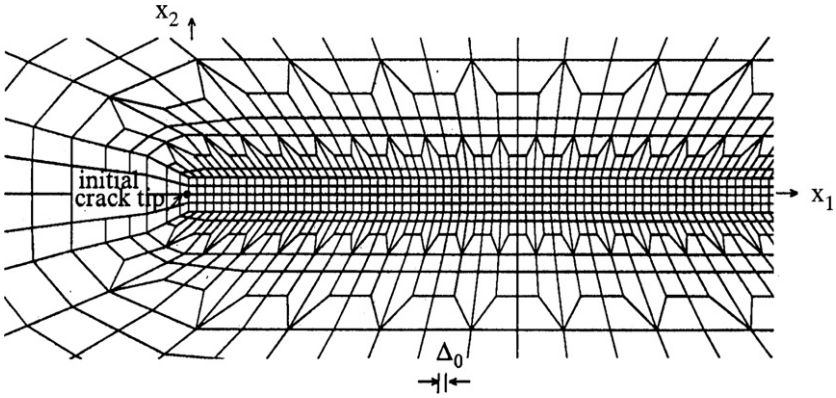

Fig. 2. Mesh used for some of the crack growth analyses.

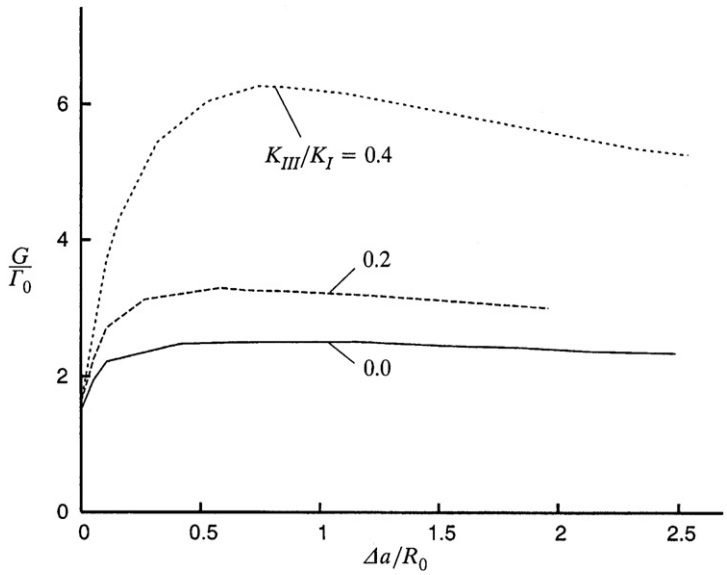

Fig. 3. Crack growth resistance curves for $T/\sigma_Y = -0.5$, $N = 0.1$ and $\hat{\sigma}/\sigma_Y = 2.4$, with different values of K_{III}/K_I.

the amount of crack growth Δa, normalised by Γ_0 and R_0, respectively. The lowest fracture toughness occurs for $K_{III} = 0$, and the fracture toughness increases significantly as the value of K_{III}/K_I is increased (the behaviour is symmetric so that negative or positive values of K_{III} give identical curves). The data points used to plot these resistance curves are taken out with rather large spacing, so they do not clearly illustrate the fact that crack growth starts when $G = \Gamma_o$.

If the energy release rate approaches a final plateau, the corresponding value is called the steady state toughness G_{ss}. This situation is approached for the two lower curves in Fig. 3, whereas the highest curve shows a clear maximum in the vicinity of $\Delta a/R_o \approx 0.7$. The highest curve is expected to reach a steady state level at some stage, but the computation has not been continued far enough to determine this level. The values to be shown subsequently are calculated as the maxima G_{max}/Γ_o of the corresponding crack growth resistance curves. The highest curve in Fig. 3 has been recomputed with twice as fine mesh in both coordinate directions near the crack-tip, which increases the maximum value a little but fully maintains the shape of the curve.

Fig. 4 shows variations of the toughness G_{max}/Γ_o vs. K_{III}/K_I for $\hat{\sigma}/\sigma_Y = 2.4$, as in Fig. 3, but for different values of the T-stress. The curve for $T/\sigma_Y = -0.5$ contains the points corresponding to the maxima of the resistance curves in Fig. 3. In addition, the figure shows a curve for $T/\sigma_Y = -0.8$, where the fracture toughnesses are significantly higher, and curves for $T/\sigma_Y = 0.0$ and $T/\sigma_Y = +0.5$, where the fracture toughnesses are lower. In all cases the value of G_{max}/Γ_o increases as the value of K_{III}/K_I is increased. Thus, for a given value of T/σ_Y and for given values of the cohesive zone model parameters the fracture toughness is increased when a mode III load is applied in addition to the mode I load. It is well known that a positive T-stress has little effect on the fracture toughness, and for $K_{III} = 0$ the values on the two lower curves are nearly identical. In the case of $T/\sigma_Y = +0.5$ the fracture toughness is nearly unaffected by K_{III} at lower values of K_{III}/K_I, but then grows a little at the end of

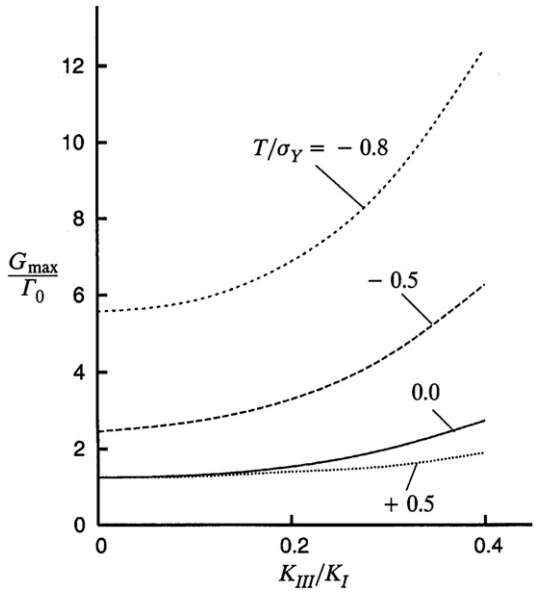

Fig. 4. Maximum fracture toughness as a function of K_{III}/K_I, for four different levels of T-stress. The curves are obtained for $\hat{\sigma}/\sigma_Y = 2.4$ and $N = 0.1$.

the curve. The values at $K_{III} = 0$ in Fig. 4 are directly comparable with some results in Tvergaard and Hutchinson (1994), but the values in Fig. 4 are a little higher. It has been found by re-running the programme from 1994 with a much finer mesh that the results agree.

The computations show that the plastic zone size around the crack-tip is much increased when a mode III load is added to the mode I load, and this appears to be the main reason why the toughness increases. Indeed, an increased size of the plastic zone was earlier found (Tvergaard and Hutchinson, 1992) to be the main reason why high values of $\hat{\sigma}/\sigma_Y$ give a fracture toughness well above the reference value, and also the increased toughness due to a negative T-stress is followed by an increased plastic zone size (Tvergaard and Hutchinson, 1994). Fig. 5 shows contours of the effective plastic strain ε_e^P, which is found by integration of the incremental expression $\dot{\varepsilon}_e^P = (2\dot{\eta}_{ij}^P \dot{\eta}_P^{ij}/3)^{1/2}$, to illustrate the plastic zone size in four different cases at stages where the resistance curves have just reached their peak value. The intensity of plastic deformation as well as the size of the plastic zone is important when comparing plastic dissipation. It is noted in Fig. 5 that the region with $\varepsilon_e^P > 0.01$

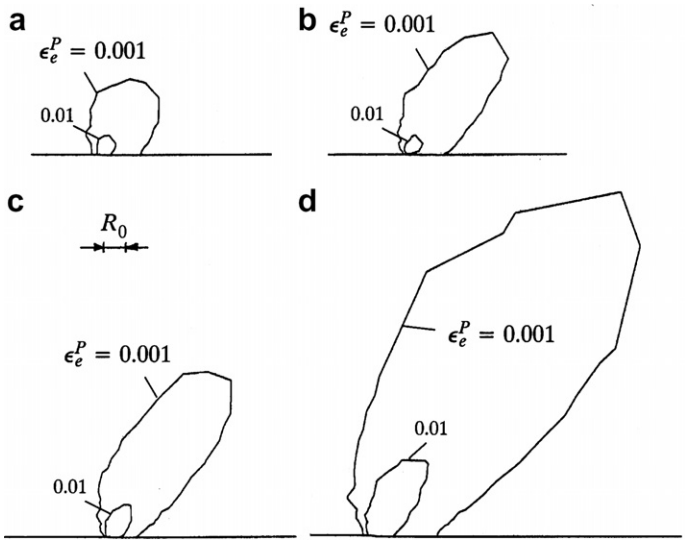

Fig. 5. Contours of the effective plastic strain ε_e^P illustrating the plastic zone size at the peak of the resistance curves. (a) At $T/\sigma_Y = 0.0$ and $K_{III}/K_I = 0.4$. (b) At $T/\sigma_Y = -0.5$ and $K_{III}/K_I = 0.0$. (c) At $T/\sigma_Y = -0.5$ and $K_{III}/K_I = 0.2$. (d) At $T/\sigma_Y = -0.5$ and $K_{III}/K_I = 0.4$.

grows when the region with $\varepsilon_e^p > 0.001$ grows, and therefore it appears that the size of the latter region gives an indication of the amount of plastic dissipation.

Fig. 5a corresponds to the curve for $T/\sigma_Y = 0.0$ in Fig. 4, at the point where $K_{III}/K_I = 0.4$, while Fig. 5b to d correspond to the curve for $T/\sigma_Y = -0.5$ in Fig. 4, at three different values, 0.0, 0.2 and 0.4, of K_{III}/K_I. The values of the fracture toughnesses in Fig. 5a and b are nearly equal, but in the first case the toughness has been increased by adding K_{III} for $T = 0$, while in the second case the toughness has been increased by adding a negative T-stress for $K_{III} = 0$. The plastically strained region is taller in Fig. 5b, but the sizes of these two regions are rather similar while the shapes differ a great deal. In Fig. 5c and d the toughness is further increased relative to that in Fig. 5b by considering non-zero values of K_{III}. In these two figures the shapes of the plastically strained regions are similar to that in Fig. 5b, and it is seen that the sizes of the regions increase significantly when the value of K_{III}/K_I is increased. The plastic regions shown in Fig. 5 are only the upper part, but the lower part has the same shape with full symmetry about the crack plane.

For $T/\sigma_Y = -0.5$ Fig. 6 illustrates the dependence on $\hat{\sigma}/\sigma_Y$ and on K_{III}/K_I. Thus, the curve for $\hat{\sigma}/\sigma_Y = 2.4$ is repeated from Fig. 4. The general trend in Fig. 5 that the fracture toughness increases for increasing value of $\hat{\sigma}/\sigma_Y$ is as expected based on the previous investigations. But Fig. 6 also shows that the increase of the fracture toughness is much larger when a mode III load is applied in addition to the mode I load. The lowest curve in Fig. 6, for $\hat{\sigma}/\sigma_Y = 1.6$, is in the range where plasticity has only a small effect on the fracture toughness. For this curve it is seen that between $K_{III}/K_I = 0.0$ and $K_{III}/K_I = 0.2$ there is hardly any effect of the mode III load, and for larger values there is only a very small effect.

The influence of an increased hardening level for the elastic–plastic material is investigated in Fig. 7 by considering curves for $N = 0.2$, still for $T/\sigma_Y = -0.5$ as in Fig. 6. In the absence of a T-stress it was already known from Tvergaard and Hutchinson (1992) that the higher hardening gives much lower fracture toughness, for the same parameter values in the cohesive zone model used to characterize the fracture process. The same effect was found with a T-stress (Tvergaard and Hutchinson, 1994). In Fig. 7 the three lower curves correspond to values of $\hat{\sigma}/\sigma_Y$ that were also considered in Fig. 6, and it is seen that the fracture toughnesses for $N = 0.2$ are much lower than those for $N = 0.1$, in the whole range of K_{III}/K_I values considered. The highest cohesive zone strength considered, $\hat{\sigma}/\sigma_Y = 3.6$, results in about the same fracture toughness at $K_{III}/K_I = 0.0$ as that found for $\hat{\sigma}/\sigma_Y = 2.8$ in Fig. 6, but at $K_{III}/K_I = 0.4$ the toughness is much lower on the highest curve in Fig. 7 than that on the highest curve in Fig. 6.

A reduced level of strain hardening is considered in Fig. 8, where $N = 0.05$. This gives much increased fracture toughness, since the low hardening material makes it more difficult to reach the stress levels necessary to make the crack grow for a given value of the cohesive zone strength $\hat{\sigma}/\sigma_Y$. The highest curve in Fig. 8 corresponds to $\hat{\sigma}/\sigma_Y = 2.4$. The same value of $\hat{\sigma}/\sigma_Y$ gives the second lowest curve in Fig. 7 for $N = 0.2$, while the curve for $\hat{\sigma}/\sigma_Y = 2.4$ in Fig. 6 shows fracture toughnesses in between the corresponding curves for the higher or lower levels of strain hardening.

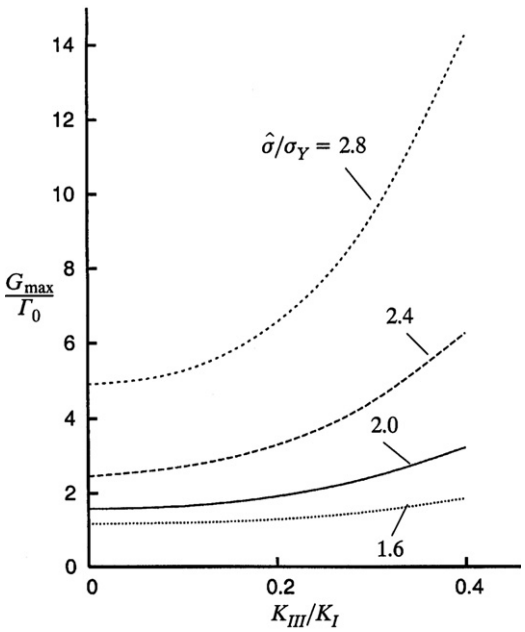

Fig. 6. Maximum fracture toughness as a function of K_{III}/K_I, for four different values of $\hat{\sigma}/\sigma_Y$. The curves are obtained for $T/\sigma_Y = -0.5$ and $N = 0.1$.

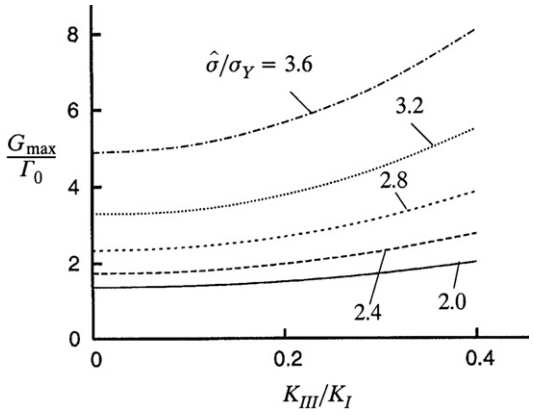

Fig. 7. Maximum fracture toughness as a function of K_{III}/K_I, for five different values of $\hat{\sigma}/\sigma_Y$. The curves are obtained for $N = 0.2$ and $T/\sigma_Y = -0.5$.

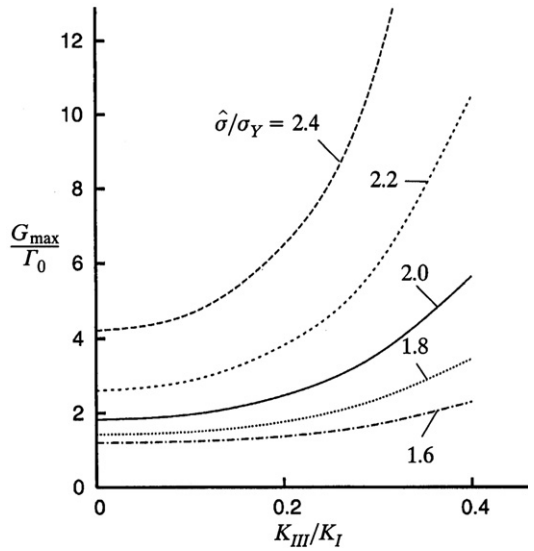

Fig. 8. Maximum fracture toughness as a function of K_{III}/K_I, for five different values of $\hat{\sigma}/\sigma_Y$. The curves are obtained for $N = 0.05$ and $T/\sigma_Y = -0.5$.

5. Discussion

For a crack in a homogeneous elastic–plastic material under standard mode I loading the present investigation considers the effect of also applying two other load systems, a T-stress and a mode III loading. Cracks in elastic–plastic materials under mixed mode I and mode III loading have been analyzed previously by a number of authors. Thus, Pan and Shih (1990, 1992) have focused on the near-tip fields of stationary cracks in power-law hardening materials and have compared their degree of singularity with the HRR singularity for a number of different mode mixities. Ductile crack growth in mixed mode I/III has been analyzed by Gao and Shih (1998) where the failure mechanism is void growth, and these authors have found some cases where the fracture toughness is reduced in the presence of a mode III component, corresponding to slanted crack growth in a plate specimen. It is noted that in the present analyses, as in Gao and Shih (1998), the possibility of a slanted crack is excluded, but they argue that a slanted crack in a plate under mode I loading will in fact experience mixed mode I/III at the crack front.

The present predictions of fracture toughness, with the fracture process represented in terms of the cohesive zone model and the ductile metal modelled as elastic–plastic, are much dependent on the evolution of a plastic zone at the current crack-tip. If no plasticity occurs, it is found that neither a T-stress nor an additional mode III loading will add to the fracture toughness. But in the presence of plastic flow the results show that increasing K_{III} for given values of K_I and T, or increasing $(-T)$ for given values of K_I and K_{III}, leads to an increased size of the plastic region (e.g., see Fig. 5). The corresponding values of the fracture toughness show that the increased size of the plastic region is accompanied by an increased fracture toughness. It is also clear from the present results that when the fracture toughness is already increased by the presence of a negative

T-stress, it will be further increased by superposing a non-zero mode III load. Predictions for a positive T-stress (Fig. 4) confirm that positive values of T have practically no influence on the toughness.

It is noted that the values of T considered here are well within the range that allows for small scale yielding. Thus, the absolute value of T does not exceed the value $2\sigma_Y/\sqrt{3}$ that would result in full scale yielding in uniaxial plane strain tension before any mode I or mode III loading was applied.

Predictions for a higher level of strain hardening (Fig. 7) or for a lower level of strain hardening (Fig. 8) show that the fracture toughness is strongly dependent on strain hardening. An increased strain hardening gives higher stress levels in the elastic–plastic region, which makes it easier to advance the crack in a cohesive zone with a fixed value of the peak stress $\hat{\sigma}$. Correspondingly, a reduced strain hardening makes it more difficult to reach the stress levels needed to advance the crack.

References

Betegon, C., Hancock, J.W., 1991. Two-parameter characterization of elastic–plastic crack-tip fields. J. Appl. Mech. 113, 104–110.

Cao, H.C., Evans, A.G., 1989. An experimental study of the fracture resistance of biomaterial interfaces. Mech. Mater. 7, 295–304.

Du, Z.-Z., Hancock, J.W., 1991. The effect of non-singular stresses on crack-tip constraint. J. Mech. Phys. Solids 39, 555–567.

Gao, X., Shih, C.F., 1998. A parametric study of mixed-mode I/III ductile fracture in tough materials under small scale yielding. Eng. Fract. Mech. 60, 407–420.

Hancock, J.W., Reuter, W.G., Parks, D.M., 1991. Constraint and toughness parameterized by T. ASTM Symposium on Constraint Effects in Fracture, Indiannapolis.

Hutchinson, J.W., 1973. Finite strain analysis of elastic–plastic solids and structures. In: Hartung, R.F. (Ed.), Numerical Solution of Nonlinear Structural Problems. ASME, New York, p. 17.

Larsson, S.G., Carlsson, A.J., 1973. Influence of non-singular stress terms and specimen geometry on small-scale yielding at crack tips in an elastic–plastic material. J. Mech. Phys. Solids 21, 263–277.

Liechti, K.M., Chai, Y.S., 1992. Asymmetric shielding in interfacial fracture under in-plane shear. J. Appl. Mech. 59, 295.

Needleman, A., 1987. A continuum model for void nucleation by inclusion debonding. J. Appl. Mech. 54, 525–531.

O'Dowd, N.P., Shih, C.F., 1991. Family of crack-tip fields characterized by a triaxiality parameter – I. Structures of fields. J. Mech. Phys. Solids 39, 989–1015.

O'Dowd, N.P., Shih, C.F., 1992. Family of crack-tip fields characterized by a triaxiality parameter – II. Fracture applications. J. Mech. Phys. Solids 40, 939–963.

O'Dowd, N.P., Stout, M.G., Shih, C.F., 1992. Fracture toughness of alumina/niobium interfaces: experiments and analyses. Philos. Mag. A66, 1037.

Pan, J., Shih, C.F., 1990. Elastic–plastic analysis of combined mode I and III crack-tip fields under small-scale yielding conditions. J. Mech. Phys. Solids 38, 161–181.

Pan, J., Shih, C.F., 1992. Elastic–plastic analysis of combined mode I, II and III crack-tip fields under small-scale yielding conditions. Int. J. Solids Struct. 29, 2795–2814.

Rice, J.R., 1974. Limitations to the small scale yielding approximation for crack tip plasticity. J. Mech. Phys. Solids 22, 17–26.

Scheider, I., Brocks, W., 2003. The effect of the traction separation law on the results for cohesive zone crack propagation analyses. Key Eng. Mater., 251–252:313-318.

Tvergaard, V., 1990. Effect of fibre debonding in a whisker-reinforced metal. Mater. Sci. Eng. A125, 203–213.

Tvergaard, V., 2001. Resistance curves for mixed mode interface crack growth between dissimilar elastic–plastic solids. J. Mech. Phys. Solids 49, 2689–2703.

Tvergaard, V., Hutchinson, J.W., 1992. The relation between crack growth resistance and fracture process parameters in elastic–plastic solids. J. Mech. Phys. Solids 40, 1377–1397.

Tvergaard, V., Hutchinson, J.W., 1993. The influence of plasticity on mixed mode interface toughness. J. Mech. Phys. Solids 41, 1119–1135.

Tvergaard, V., Hutchinson, J.W., 1994. Effect of T-stress on mode I crack growth resistance in a ductile solid. Int. J. Solids Struct. 31, 823–833.

Tvergaard, V., Hutchinson, J.W., 2008. Mode III effects on interface delamination. J. Mech. Phys. Solids 56, 215–229.